Preserved Neural Dynamics across Arm- and Brain-controlled Movements

Running Title: Emerged neural evolution in feedforward BMI

Chenyang Li[1, 2, 3], Xinxiu Xu[1, 2], Tianwei Wang[2, 3], Yun Chen[1, 2], Cong Zheng[1, 2], Yiheng Zhang[3], Qifan Wang[3], and He Cui[1, 2, *]

1. Beijing Institute for Brain Research, Chinese Academy of Medical Sciences & Peking Union Medical College, Beijing, 102206, China
2. Chinese Institute for Brain Research, Beijing, 102206, China
3. Center for Excellence in Brain Science and Intelligence Technology, Institute of Neuroscience, Chinese Academy of Sciences, Shanghai 200031, China

*Correspondence: hecui@cibr.ac.cn

Abstract

The neural response for motor control is complex and dynamic; it has been found to dramatically transit from planning to executing movements. As brain-machine interfaces (BMIs) can directly connect the brain and the external world by yielding comparable motor outcomes with artificial apparatus, a central question remains whether the neural dynamics underlying brain-control movement share characteristics or mechanism in natural neural motor control. To enable a systematic comparison, we developed a feedforward BMI framework that enables rapid cursor control to intercept moving targets. This BMI allowed monkeys to voluntarily initiate neural states which controlled the direction and timing of a launched ballistic movement, like skeet shooting. Based on this, we found similar neural representation patterns and computational structure across brain- and arm-control conditions. Notably, in addition to resembling the rotational structure in natural reaching, the neural population dynamics during open loop control also shared preserved manifold with those during arm interception. These findings suggest a fundamental principle and reveal a set of basic computational motifs, for neural control of movement in an abstract hierarchy independent of constraints from actuators. This study thus has potential to reshape the consideration of how BMIs assist paralyzed patients in interacting with dynamic environments and promote next-generation BMI systems.

Introduction

Brain-machine interface (BMI) enables an alternative way for the brain to interact with the external world. By decoding neural signals in real-time, BMI has succeeded in replacing lost motor function (Bensmaia & Miller, 2014; Gilja et al., 2012; Lebedev & Nicolelis, 2017; Pandarinath & Bensmaia, 2022; Velliste et al., 2008). In recent years, a growing body of work shows that many sensorimotor processes engaged during able-bodied movement are also recruited during BMI control (Golub et al., 2015; Stavisky et al., 2017). These parallels support the notion that high-performing BMI may rely on sensorimotor processes similar to those underlying natural motor control (Stavisky et al., 2017), thereby motivating broader applications of dynamical preservation in BMI design. Nevertheless, there remains no direct evidence demonstrating that the neural mechanisms supporting these cognitive processes are preserved between natural movement and BMI control.

Recent decades have seen a shift from seeking explicit movement-parameters representations to population-level, dynamical-systems accounts of cortical movement control (Churchland & Shenoy, 2024). In this view, motor cortex acts as a pattern generator whose neural dynamics are initialized by preparatory activity and evolve autonomously during motor execution (Shenoy et al., 2013). These prominent dynamical features of natural movements potentially reflect a shared principle across movement types and fundamental properties of the neural basis of behavior. Given its explanatory power, dynamical system perspective-based modeling has also shown preliminary success in improving human BMI control of assistive devices (Kao et al., 2015; Pandarinath et al., 2018). However, most BMIs built on iterative feedback control remain far from biomimetic in design, which may limit their ability to fully harness the performance gains offered by the dynamical-systems framework.

In the present study, we designed a feedforward BMI that enables monkeys to control a computer cursor through self-paced, ballistic movement trajectories, allowing them to intercept rapidly moving targets. This BMI framework features clearly defined preparation and execution epochs, as well as an epoch-switch detector allowing for self-paced movement initiation. Strikingly, neural responses during this biomimetic brain-control process exhibited the prominent dynamical features observed during naturalistic arm reaching and they occupied the same low-dimensional neural manifold, suggesting that similar neural dynamics underlie both brain-controlled and arm movements. Our study provides direct evidence that neural dynamics are preserved across BMI and natural movement, offering not only a platform for developing universal BMI but also a more ideal reduced system for investigating sensorimotor control.

Feedforward BMI for intercepting moving target

Given their shared neural basis and similar task demands, it is reasonable to anticipate that neural activity during BMI and natural movement would align within the same low-dimensional neural manifold constrained by evolutional circuit and behavioral experience (Perich et al., 2025). We hypothesize that, with appropriate biomimetic design, the latent states in both BMI and natural reaching would trace similar trajectories on the shared manifold, progressing from the preparatory subspace to the execution subspace, reflecting the characteristic initial-state–dependent evolution of cortical dynamics (Shenoy et al., 2013) (**Fig. 1a**).

To test this hypothesis, we proposed a feedforward BMI framework with the following key features (**Fig. 1b**). (1) Clearly delineated preparation and execution epochs. During the preparation epoch, a decoder enables subjects to initialize neural states either implicitly or explicitly with visual feedback. During the execution epoch, the initial state determines the launch direction of a ballistic movement with a bell-shaped speed profile in a feedforward manner. Additional feedback-based adjustments, implemented using the same decoder, can be incorporated to provide necessary online corrections. (2) A detector or "gate" separates the two epochs and acts as a movement-onset trigger. Crucially, the gate's activation is determined by the subject's own intent, rendering the BMI asynchronous, as movement initiation is detected directly from neural intention.

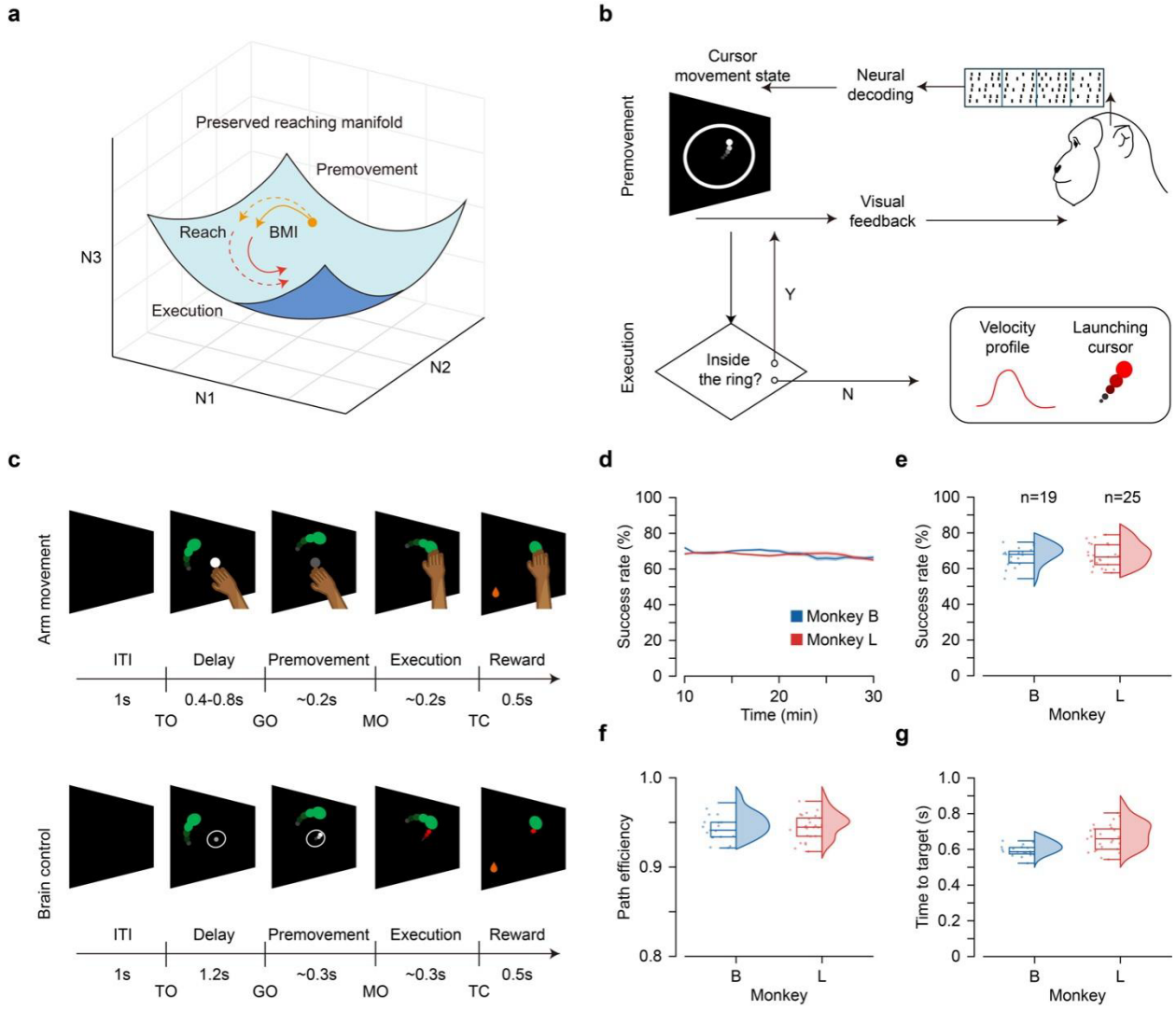

Figure 1 The feedforward BMI and its performance. *(a) Hypothesis for preserved neural principle across brain- and arm-controlled movement. We supposed that the reaching-like dynamics would emerge with the explicitation of feedforward control in this BMI because of the intrinsic properties of the motor cortex. (b) The schematic diagram of the feedforward BMI framework. This BMI is featured by distinct premovement and execution epochs. In the former epoch, the cursor is brain-controlled to exceed a threshold in a closed-loop way. When the cursor crosses the threshold, it switches to the next epoch, i.e., the cursor launches ballistically*

in an open-loop way. (c) The interception task including arm- and brain-controlled conditions.TO: target on, GO: GO-cue on, MO: movement onset, and TC: touch target (d) Success rates in an example session. The first 10 minutes of each session were used for decoder calibration. A sliding window of 75 trials was used and the step was 1 trial. (e) Overall success rates in brain-controlled sessions. (f) Path efficiency of cursor trajectories in brain-controlled sessions. (g) Time to target (duration from the onset of cursor control to the successful interception) in brain-controlled sessions.

As an instantiation of such biomimetic BMI framework, we recorded neural activity from two microelectrodes implanted in the primary motor cortex (M1) and dorsal premotor cortex (PMd) of monkey B and L (**Fig. S1**). Monkeys were firstly trained to perform a delayed center-out reach task manually on the vertical touchscreen with target either static or moving, which is referred as manual task (**Fig. 1c**). Previous studies have shown that intercepting moving targets requires precise coordination of movement direction and timing, making it a suitable task for evaluating BMI performance (Li et al., 2018; Zhang et al., 2025). We used a target speed of ±120°/s in recording sessions, which is appropriate for most monkeys. For the BMI task, we first calibrated a velocity decoder using threshold-crossing firing rates recorded while the monkey passively observed a computer-controlled cursor performing center-out movements. Then, the monkey, with its arm restrained in the chair, was trained to control the cursor in a closed-loop decoder adaptation manner (Gilja et al., 2012; Orsborn et al., 2014) until computer assistance was removed and performance exceeded 80% success. Next, we introduced a white 'threshold ring' at the center. After a 1-sec delay period in which target was displayed, the monkey could move the cursor appeared at the center. Once the cursor crossed the ring, it was launched centrifugally along the radial direction of the crossed point, following a straight trajectory with a fixed bell-shaped speed profile, whose initial velocity matched the cursor speed at ring crossing. We defined the period during which cursor remained inside the ring as the "premovement" epoch, corresponding to the reaction-time period in the manual task. If the cursor entered a 5-cm radius around the target, a reward was delivered. If the cursor overshot and missed the target, the monkey was allowed to control the cursor using visual feedback. If the target was not reached within the following 1 s, the trial was marked as a failure, and no reward was given (**Fig. S2a and S2d**).

After about two weeks of training, both monkeys successfully learned to perform the BMI task within the feedforward BMI framework. Task performance remained stable throughout each session (**Fig. 1d**), with mean success rates near 70% (monkey B: 66.8±2.6% across 19 sessions, monkey L: 66.9±2.6% across 25 sessions, mean±1.96 SEM) (**Fig. 1e**). In most of the successful trials, the cursor traveled directly toward the target without requiring any feedback-based corrections. The averaged path efficiencies were 0.94±0.007 for monkey B and 0.96±0.006 for monkey L (**Fig. 1f**). The time from the cursor initiation to target acquisition (time to target) was 0.59 ± 0.015 s for monkey B and 0.66 ± 0.03 s for monkey L, comprising approximately 0.31 ± 0.005s and 0.37 ± 0.026 s in the premovement epoch and 0.28 ± 0.011 s and 0.30 ± 0.012 s in the execution epoch (**Fig. 1g**), comparable to values observed in the manual task. As in the manual task, movement trajectories were uniformly distributed across directions in the BMI task, indicating no reach directional bias (**Fig. S2b-f**). For subsequent analyses, trials were grouped into eight reach directions evenly spaced at 45° intervals.

Feedforward BMI reproduced across-epoch change in neural representation

To investigate whether the feedforward BMI task resembles the manual task, we first analyzed single-unit responses. As in the manual task, neurons during the BMI task also exhibited sequence-like firing patterns characteristic of natural reaching, albeit with reduced temporal sparsity (**Fig. S3**). We fit each unit's activity with a cosine tuning model and quantified the percentage of units with a goodness of fit greater than 0.7 (tuned units' percentage, TU%). During the inter-trial interval (ITI), TU% of was near zero for both tasks (**Fig. 2a-b**). Following target onset, TU% began to rise in both tasks, though the increase in the BMI task was delayed and slower compared with the manual task, indicating a gradual engagement of neural population. During the premovement epoch, TU% reached a plateau that was comparable across tasks for monkey B but slightly lower in the BMI task for monkey L, likely reflecting sampling bias in recorded neurons. Notably, during the execution epoch when the cursor moved without direct brain control, TU% in the BMI task remained similar to that in the manual task (51.2 $\pm$ 3.1% for monkey B; 44.3 $\pm$ 2.5% for monkey L). To rule out the effect of visual feedback, we further occluded the cursor during flight so that it was invisible to the monkey. Even under this condition, TU% remained high in the execution epoch (**Fig. S4**). Given that the cursor motion directly determined reward outcome and that monkeys were afforded an opportunity to correct potential target misses, the sustained TU% observed during the execution epoch suggests that monkeys were still actively engaged in the open-loop process, rather than passively observing the cursor's ballistic motion.

We further characterized the neural representation pattern by computing each neuron's preferred direction (PDs, Georgopoulos et al., 1982). During natural reaching, a neuron's PD is typically stable within either the preparatory or execution period but shifts between the two (Suway et al., 2018). Here, we defined a neuron as exhibiting a "PD shift" if the angular difference between PDs of two epochs exceeded 90°. As expected, neurons in both tasks exhibited varying degrees of PD shift from premovement to execution epoch (**Fig. 2c-f**). Changes in modulation depth and baseline from the premovement to execution epochs were also comparable across task, further supporting a similar across-epoch representational transitions (**Fig. S5**). The proportion of PD-shift neurons in the tuned units increased over time (**Fig. 2g, i**). In the manual task, this increase began ~0.4 s before movement onset (MO), whereas in the BMI task the ramping began 0.1–0.2 s later. The overall fraction of PD-shift units was consistently lower in the BMI task than in the manual task (execution-epoch plateau: 36.1% in manual task and 32.7% in BMI task for monkey B; 43.4% and 22.7% for monkey L). As expected for a continuous preparatory process, the PD shift from the delay to premovement epoch in the manual task was smaller than the shift from delay to execution epoch (**Fig. 2h, j**). Strikingly, this relationship was preserved in the BMI task. This indicates that the delay epoch when cursor is static and premovement epoch when cursor was controlled via visual feedback form a continuous neural process, whereas the transition from premovement to execution epoch reflects a genuine shift in neural dynamics.

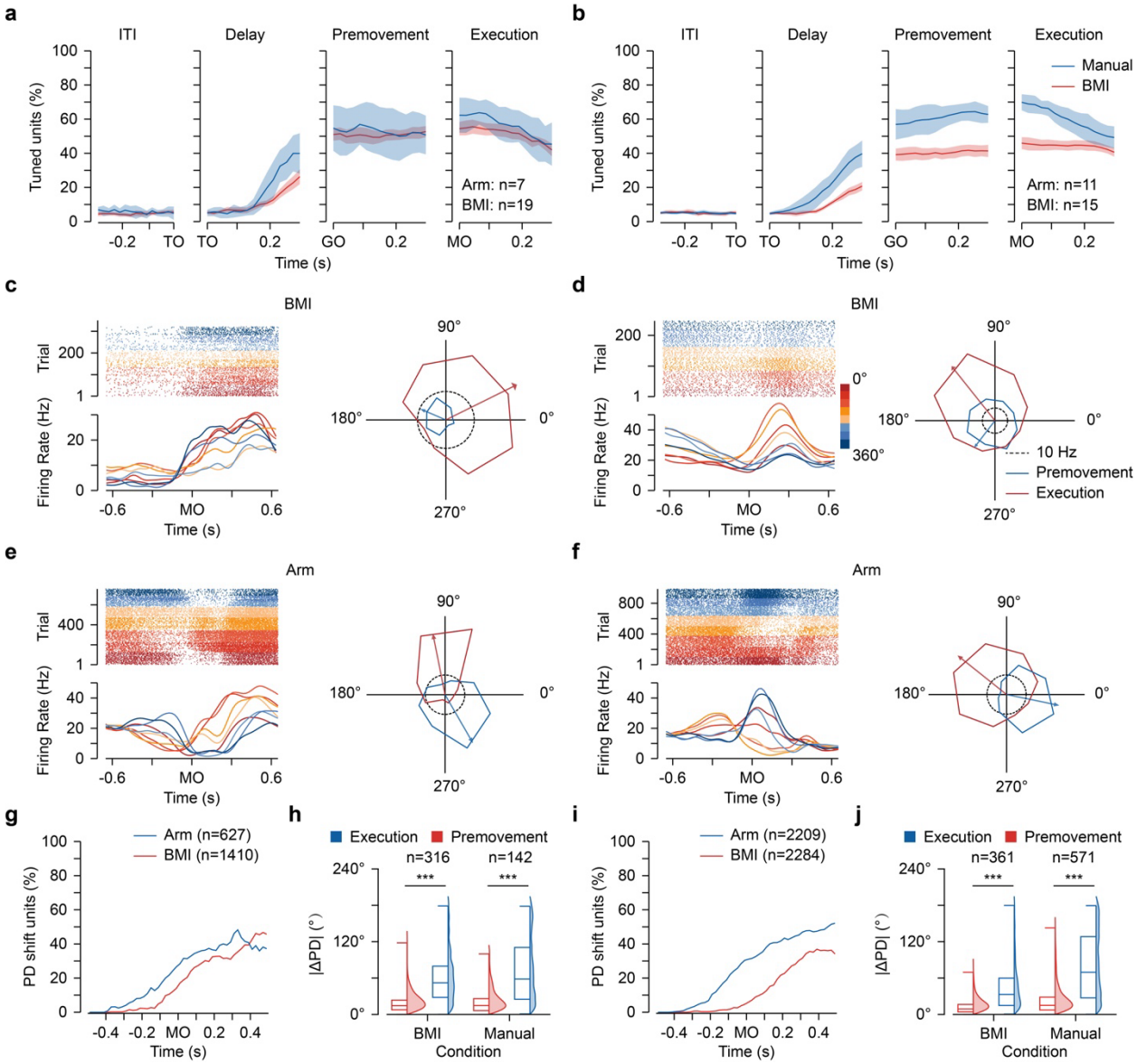

Figure 2 Single-neuron tunings to arm- and brain-control movements. *Left panel for monkey B and right panel for monkey L. (a-b) Tuned unit's percent (TU%) in different epochs when aligned to target on (TO), Go-cue on (GO), and movement onset (MO) in the arm-controlled (blue) and brain-controlled (red) conditions; (c-d) Example neurons with PD shift in the arm-controlled condition; On the left are the raster plot and peri-event time histogram (PETH), aligned to MO. Different colors represent different movement directions. On the right is a polar plot, where the angle denotes the movement direction, the radius denotes the averaged firing rate in the corresponding direction, and the arrow shows the preferred direction in the certain epoch. Premovement epoch: -200 ms to -180 ms from MO; Execution epoch: 180 ms to 200 ms from MO. (e-f) Example neurons with PD shift in brain-controlled condition. (g, i) The proportion of 'PD shift' neurons over time relative to MO. Criteria for 'PD' neurons: goodness-of-fit of the cosine tuning model was greater than 0.7 both in 0.5 s before MO and the current time. Criteria for 'PD shift' neurons: the difference between current PD and the PD in 0.5 s before MO exceeded 90°. (h, j) Absolute differences of PD between premovement and delay epochs (red) and between execution and delay epochs (blue) in both conditions.*

Feedforward BMI resembled neural population activity pattern in arm movement

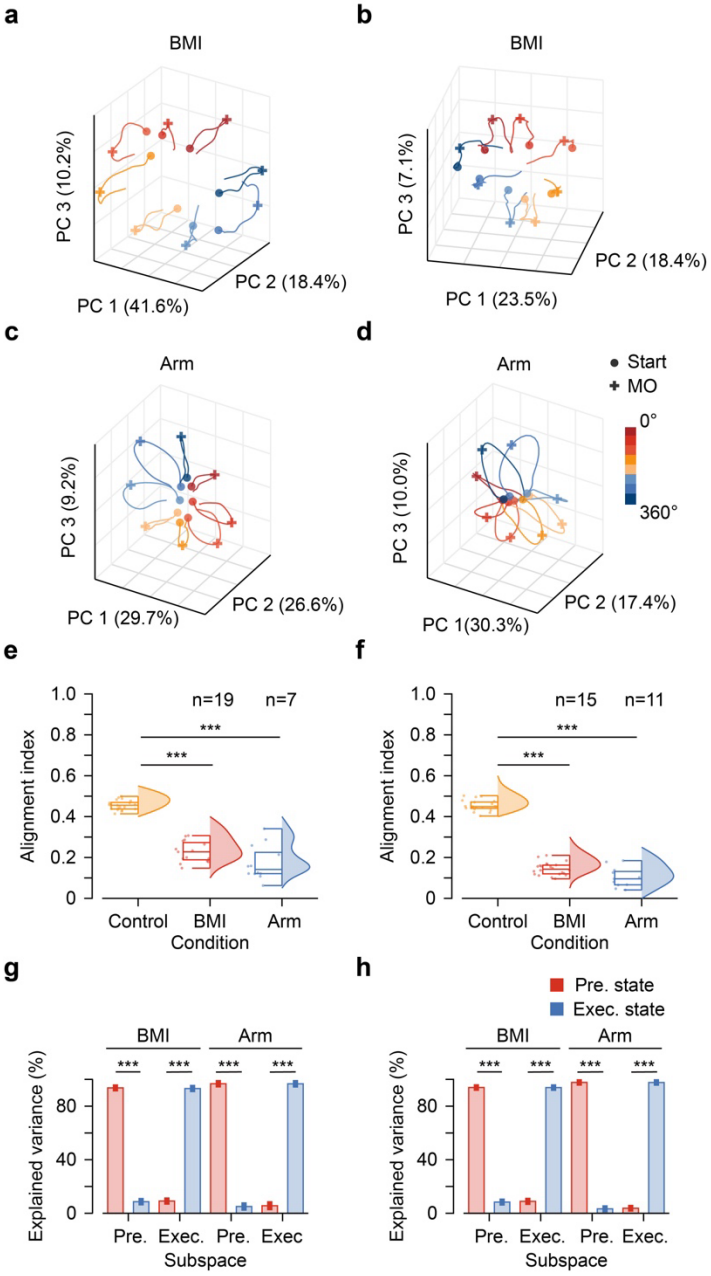

Figure 3. Neural state transition from the planning to execution epochs revealed by dimensionality reduction. *Left panel for monkey B and right panel for monkey L. (a-d) Neural trajectories of the top three principal components (PCs) identified with principal component analysis (PCA) in the BMI and arm-controlled condition. Different colors represent distinct arm movement directions (a-b) or cursor's ballistic directions (c-d). (e-f) Alignment index in the arm- and brain-controlled movements. Bars of 'control' correspond to the indexes expected from random dimensions. (g-h) Percentage of the premovement-epoch data variance and execution-epoch data variance explained by the top six execution-epoch PCs or premovement-epoch PCs in the arm- and brain-controlled conditions.*

Given the similar single-unit firing patterns observed across tasks, we next asked whether our feedforward BMI also reproduces the population-level dynamics characteristic of natural arm movements. In three-dimensional subspaces constructed from trial-averaged population data using principal component analysis (PCA), neural trajectories from the BMI and manual task exhibited two common features: first, the neural trajectories were ordered according to movement direction; second, although trajectories initially evolved outward from the origin, they reversed direction inward shortly after MO, transitioning from the premovement to the execution epoch (**Fig. 3a-d**). Examining individual principal components (PCs) revealed that this trajectory reversal at MO was primarily driven by the third PC (PC3), which showed a value flip for all movement directions, whereas PC1 and PC2 remained relatively stable over time (**Fig. S6**). The shared neural geometry verified the PD-shift phenomenon observed at single-unit level and further indicates that our feedforward BMI preserves a key computational structure underlying natural arm movements.

Orthogonality between preparatory and execution neural subspaces is another key phenomenon observed during ballistic arm movements (Elsayed et al., 2016). To assess whether this property was also present in our BMI framework, we first quantified the extent of subspace overlap using the alignment index, defined as the fraction of execution-epoch variance captured by the premovement-epoch subspace spanned by the top ten PCs (Elsayed et al., 2016). Perfect orthogonality would yield an alignment index of zero. Consistent with previous findings, the alignment index for the manual task was near zero and significantly lower than the control level derived from simulated random data (**Fig. 3e, f**, 0.173 ± 0.053 for monkey B; 0.102 ± 0.033 for monkey L). As expected, the alignment indices of the BMI task were comparable to those of the manual task (0.228 ± 0.029 for monkey B; 0.145 ± 0.014 for monkey L). We further identified the 'premovement subspace' and 'execution subspace' and projected neural activity from each epoch into these subspaces, following prior methodology. In both the BMI and tasks, each subspaces captured high variance within its corresponding epoch but minimal variance from the other epoch (**Fig. 3g, h**), indicating strong orthogonality between preparatory and execution dimensions. These results demonstrate that our feedforward BMI has well-defined preparatory and executing periods which recapitulate critical dynamical features observed during the ballistic arm movement.

Feedforward BMI inherited evolution rule and neural manifold from arm movement

Neural population dynamics often evolve in a quasi-oscillatory manner across movement types, providing direct evidence for the computational mechanisms underlying cortical dynamics (Churchland et al., 2012). To examine whether this principle is also preserved in the feedforward BMI, we applied jPCA to neural activity pooled across sessions (-100 to 300 ms around MO). Consistent with previous studies, neural dynamics in the manual task exhibited clear rotational structure (**Fig. 4a-d**). Remarkably, a similar rotational pattern was also present in the BMI task, indicating that the same underlying dynamical rule is preserved during biomimetic brain control.

Given the preceding findings, we finally asked whether the BMI and manual task shared a low-dimensional latent dynamics, i.e. a common neural manifold. To identify potential shared neural modes, we performed canonical correlation analysis (CCA) on the top ten PCs of population data (-300 to 400 ms around MO) from pairs of sessions, either from BMI or manual task. Because neural modes were ordered by their corresponding PCs, canonical correlation naturally decreased with increasing mode index, reflecting diminishing explained variance (**Fig. 4e, f**). As expected, neural

modes from two manual-task sessions showed the highest correlations, whereas shuffled control constructed from simulated random data exhibited the lowest. Within-task correlations were lower for BMI sessions than for manual sessions, with the first three modes showed high correlation, and correlations for higher-order modes dropped sharply, suggesting that shared latent dynamics across BMI sessions were captured by fewer neural modes. Intriguingly, the correlation pattern between BMI and manual sessions resembled the within-BMI pattern, with the across-task correlations declined more steeply but remained above the shuffled level. Together, these results provide direct evidence that the BMI and manual tasks shared a preserved low-dimensional neural manifold, despite their distinct effectors.

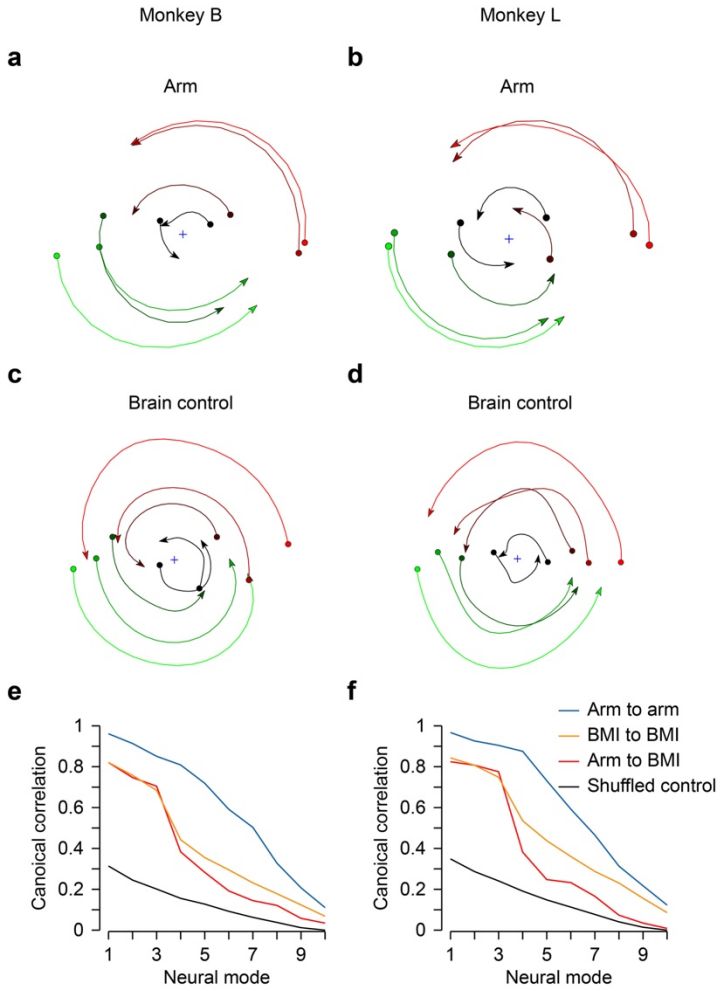

Figure 4 Neural latent dynamics during arm- and brain-controlled movement. *Left panel for monkey B and right panel for monkey L. (a-b) Projection of neural activities to jPCA space in the arm-controlled condition. Each trajectory represents one of the eight movement directions. 469 neurons were pooled for monkey B (a) and 566 neurons for monkey L (b). (c-d) Projection of neural activities onto jPCA space in the brain-controlled condition. Each trajectory also represents one of the eight movement directions. 486 neurons were pooled for monkey B (c) and 568 neurons for monkey L (d). (e-f) Correlation changing in different neural mode. The correlation for aligned neural activity in PCA space were divided to four groups: within session of arm movement (blue), brain control (brown), across sessions (red), and random trials selected from all sessions (black). The time window was set to the 300 ms before the ballistic and movement onset.*

Discussion

Biomimetic BMI can benefit from well-established motor control principles, particularly frameworks that emphasize cortical preparatory dynamics in generating future movements. Here, we proposed and implemented a biomimetic feedforward BMI architecture featuring a distinct preparatory stage-which optimizes the neural initial state-and an execution stage where the cursor moves autonomously. This design captured key dynamical features of arm movements. Specifically, our feedforward BMI demonstrated a robust shift in neural representations between the premovement (preparation) and execution epochs, clear orthogonality between the corresponding subspaces, a prominent rotational latent structure during execution, and, crucially, a preserved low-dimensional manifold shared with natural reaching. Our results provide direct evidence to the conservative neural dynamic across BMI and natural behaviors.

Extending BMI control from 2D cursors to 3D robotic devices remains challenging, often resulting in slower, less accurate movements. While evidence that latent population dynamics are preserved across time, animals, and behaviors has motivated manifold-alignment-based algorithms to address recording instability (Degenhart et al., 2020; Gallego et al., 2020; Karpowicz et al., 2025; Safaie et al., 2023), a more fundamental solution lies in biomimetic design. Our BMI architecture, which actively produces and relies on biomimetic dynamics, unifies natural and brain-controlled movement within a common sensorimotor framework. This unification is pivotal, as it directly addresses a central challenge in developing high-performance, generalizable BMIs: the prohibitive cost of collecting massive, subject-specific neural datasets for decoder training. By ensuring that the brain operates in a familiar dynamic regime during BMI control, our approach enables a novel strategy of leveraging large-scale, able-bodied neural and behavioral datasets to pre-train a foundational decoding model. For individual patients, only minimal calibration data is then needed to align their neural dynamics to this model, achieving rapid and robust personalization.

In summary, we introduced a feedforward BMI that incorporates biomimetic preparatory and execution periods, and we demonstrated that it preserves key neural dynamical features observed during arm movements. Our findings provide direct evidence that neural dynamics are preserved across BMI and natural movement. This word may not only offer a powerful framework for probing fundamental principles of sensorimotor control but might also bridge the fundamental gap between BMI and generative AI.

Methods

Experimental preparation

Two male macaque monkeys (*macaca mulata*, B and L, weighted 5-9 kg) were trained to perform manual and feedforward BMI interceptions. In each session, the animal was seated in a custom-made primate chair facing a vertical touchscreen (Elo Touchsystems, 19”; sampling at 60 Hz, spatial resolution <0.1 mm) 30 cm away. The animal was head-fixed in a primate chair via two headposts implanted into the skull along the middle seam. Hand positions were monitored by recording the location of an optically reflective marker attached to the second joint of the index finger (Vicon Inc.). Before neural recordings, animals were trained to achieve a success rate of over 90% when performing the manual interception task, in order to ensure the high efficiency in the arm movement and to help the animal comprehend the feedforward BMI interception task.

For both monkeys, two 96-channel microelectrode arrays (1.5 mm-long electrode shanks, Blackrock Microsystems) were implanted into primary motor cortex (M1) and dorsal premotor cortex (PMd). The neurosurgery for implantation was operated under anesthesia (induced by 10 mg/kg ketamine, then sustained by 2% Isoflurane). Neural activities were recorded via a Cerebus acquisition system (256-channel recording system, Blackrock Microsystems), sampled at 30 kHz.

All procedures were in accordance with NIH guidelines and were approved by the Institutional Animal Care and Use Committee (IACUC) of the Chinese Institute for Brain Research, Beijing.

Offline processing

In the present study, 34 sessions were recorded in total, including 20 sessions of brain control and 14 sessions of arm movement for monkey B, and 44 in total including 25 of brain control and 19 of arm movement for monkey L. Spikes were sorted via kilosort 2.5. The average numbers of well-isolated units for arm movement and brain control were 94 and 85, respectively, for monkey B, and 201 and 148, respectively, for monkey L.

The Kilosort2.5 algorithm was deployed in the singularity container provided by the spikeinterface and all the data was offline sorted and checked manually. The sorted neural data and behavioral data were organized as Neurodata Without Borders (NWB) data formation for the further loading and analysis with Pynapple.

Interception paradigm and feedforward BMI design

The behavioral paradigm of manual interception was the same as we recently reported (Zhang et al., 2025). At the beginning, a green circular cursor with a radius of 2.5 cm appeared in the center of the touchscreen as a cue of touching. When a touch within the central cursor was held for 300 ms, a green circular target with the same radius appeared at a random location, moving along a circular path with a radius of 12 cm around the center of the screen. Conditions in which target moved clockwise (CW: -120°/s, -240°/s) or counterclockwise (CCW: 120°/s, 240°/s), or target stayed stationary (0°/s) were pseudo-randomly interleaved trial by trial. The central cursor turned dark as a GO cue after a random delay (400-600 ms), then the monkey was required to initial an interception

within 500 ms. Once any peripheral location was touched, the target stopped. If the touch was within the target and held for 300 ms, a red circular cursor with the same radius would appear in the touched position as a cue of success and a drop of liquid food was delivered. If the touch was out of the target, a blue cursor appeared in the touch position as a cue of failure.

The behavioral paradigm in the brain-controlled condition was designed to resemble the manual paradigm except that monkey's upper limbs were restricted into the monkey chair. At first, three objects appeared in the touch screen simultaneously: a circular cursor in the screen center with a radius of 0.5 cm and changeable colors indicating whether the cursor could be driven by neural activities (gray meant uncontrollable and white meant controllable), a white ring with a radius of 2 cm located in the screen center, and a green circular target with a radius of 1.5 cm revolving in a constant circular motion (±120 deg/s) or static with a radius of 10 cm around the center. The probabilities that the target appeared with the angular velocity of 120°/s, -120°/s, or 0°/s were 0.4, 0.4 and 0.2, respectively. After one second, the cursor's color changed from gray to white, and with another delay of 0.2 second which approximately equaled monkey's reaction time the cursor could be driven by the monkey. When the cursor reached the ring, its color turned red, indicating the phase of ballistic flight without online correction, and it launched in the straight-line direction from center of the ring to the position on the ring it reached, and with a straight trajectory following a bell-shaped speed profile defined in equation (1) (Kao et al., 2021):

$$v_t = v_0 \left(\frac{t}{\tau}\right)^2 e^{-\frac{1}{2}\left(\frac{t}{\tau}\right)^2} \qquad 1$$

where v_t was the cursor's speed as t, time 0 was the moment when the cursor crossed the ring, the magnitude of v_0 was the same as that of the speed in time 0, and τ was a time constant which determined the flight duration from the ring to the peripheral circle. If the distance between the cursor and target was less than 5 cm, they both stopped for 100 ms, then a reward was delivered. If the cursor reached the peripheral circle but missed the target, its color turned white again, allowing the subject to catch up the moving target in another 1 second. If it succeeded, the cursor turned red and stopped for 100 ms then a reward was given, otherwise there was no reward.

Feedforward BMI training

A training protocol that included three steps was designed for the brain-controlled interception. In the first step, the monkey was trained to perform the center-out task via brain control in which there was a delay epoch but no ring or ballistic flight. Training began from the one-dimensional center-out task in which the target appeared only in the left or right 10 cm from the center of the screen and the cursor could be directed by neural activities horizontally. If the distance between the cursor and target was less than 5 cm, the cursor would turn red as a cue of success. It was considered as a failure if the cursor reached the edge of the screen or did not reach the target in 10 seconds. Both monkeys spent about 1-2 days to achieve an accuracy rate of over 90%, then it switched to a two-dimensional center-out task in which the target appeared in a random point on a circle with a radius of 10 cm and the requirement was the same. It took both monkeys about 3-5 days to achieve an accuracy rate of over 90% in the two-dimensional center-out task.

In the second step, the monkey was trained to perform the center-out task via the feedforward BMI in which the paradigm was similar to that of the feedforward BMI interception except that the target was static. It took both monkeys about 1-2 days to achieve an accuracy rate of over 90% in this step, then it progressed to step3 in which every session began with the two-dimensional center-out task. If the success rate was over 80% after the first minute, the task switched to the feedforward center-out paradigm. If the monkey succeeded over 80% after one minute, the task switched to the feedforward interception paradigm in which the angular velocity of target was the same as the maximum in the previous day. Every time when the success rate was over 70% after 30 minutes, 5°/s would be added to the angular velocity until its absolute value reached 120 °/s. The angular velocities of target started from 15°/s, -15°/s and 0°/s random interleaved in the first day of step 3. It took both monkeys about 14 days to finally intercept the target with the angular velocities of ±120°/s with a success rate of 70%.

Decoder initialization and calibration

The brain-control task was performed under the restriction of monkey's hands. A BMI framework for online collection of neural data, decoding and presenting decoded results was developed based on Robotic Operating System 2 (ROS2). During the initialization of the decoder, the monkey observed a white cursor move from the screen's center to a position 10 cm away with the velocity of 6 cm/s. In this stage, two asynchronous processes were used to inquire of neural data from the acquisition system and the cursor's motion state. The input of the decoder was organized into a vector as follows:

$$x_t = \left[p_t^{hori.}, p_t^{vert.}, v_t^{hori.}, v_t^{vert.}, 1\right] \quad 2$$

where x_t was the cursor's motion state at time *t*, p_t was the cursor's position, v_t was the cursor's velocity, $hori.$ and $vert.$ denoted their horizontal and vertical components, respectively. In the phase of observation, the BMI system inquired of the neural vector y_t and the vector of cursor's motion state x_t every 20 ms, paired them into a piece of data, and sent it into a buffer that could contain 500 pieces of data and followed the rules of first in and first out. The decoder was updated when there were 500 pieces of data in the buffer. In this study, recalibrated feedback intention-trained Kalman filter (ReFIT-KF, (Gilja et al., 2012) was used with the two equations:

$$\boldsymbol{x}_t = A\boldsymbol{x}_t + \boldsymbol{w}_t \quad 3$$

$$\boldsymbol{y}_t = D\boldsymbol{x}_t + \boldsymbol{u}_t \quad 4$$

where *A* was the cursor's state transition matrix $A \in \mathbb{R}^{l\times l}$, *D* was the observation matrix $D \in \mathbb{R}^{m\times l}$, l was the vector length of $\boldsymbol{x}_t$, m was the vector length of $\boldsymbol{y}_t$, $\boldsymbol{w}_t$ and $\boldsymbol{u}_t$ were the additive Gaussian noise and obeyed the Gaussian distribution with a mean of 0 and the covariance matrix of state (*W*), the covariance matrix of observation (*U*). The decoder's parameters were updated in accordance with the following equations:

$$A = X_2X_1^T(X_1X_1^T)^{-1} \quad 5$$

$$D = YX^T(XX^T)^{-1} \quad 6$$

$$U = \frac{1}{B-1}(X_2 - AX_1)(X_2 - AX_1)^T \quad 7$$

$$W = \frac{1}{B}(Y - DX)(Y - DX)^T \quad 8$$

Every piece of data in the buffer was transformed into matrix $X \in \mathbb{R}^{N\times m}$ and $Y \in \mathbb{R}^{N\times l}$, B was the number of paired $\boldsymbol{x}_t$ and $\boldsymbol{y}_t$ in the buffer. If the length in time series was T, X_1 was all the $\boldsymbol{x}_t$ in $[t_0, t_{T-1}]$, and X_2 was all the $\boldsymbol{x}_t$ in $[t_1, t_T]$. The decoder's parameters were continuously updated in an asynchronous process during the decoder's initialization and recalibration, and the initialization ended when the decoder was updated for the first time, yet yielding the suboptimal performance. An output vector was constructed as follows:

$$\boldsymbol{v}_t^{output} = \alpha \boldsymbol{v}_t^{assistant} + \beta \boldsymbol{v}_t^{decoder} \quad 9$$

where $\boldsymbol{v}_t^{output}$ was the velocity vector of output which determined the cursor's state, $\boldsymbol{v}_t^{assistant}$ was the vector of the assistance which was a unit vector and always pointed to the target, α was a manually adjusted factor, $\boldsymbol{v}_t^{decoder}$ was the decoder vector which was the output of trained Kalman filter, and β was the manually adjusted decoder gain. $\boldsymbol{v}_t^{output}$ was to make the monkey's performance above a threshold by adjusting parameters during the recalibration in which it was assumed that a movement intention pointing to the target was continuously generated by the monkey. In the phase of recalibration, the BMI system inquired of the neural vector and the movement intention at that time every 20 ms, paired them, sent it into the buffer, and kept updating the decoder simultaneously. The movement intention was computed as follows:

$$\boldsymbol{v}_t^{intention} = \left\|\boldsymbol{v}_t^{output}\right\|_2 \boldsymbol{v}_t^{target} \quad 10$$

where $\boldsymbol{v}_t^{intention}$ was the monkey's movement intention, and $\boldsymbol{v}_t^{target}$ was the unit vector pointing to the target. During the recalibration, α and β were adjusted as follows: if the success rate exceeded 90% in each minute when the monkey performed the one or two-dimensional center-out task, α would decrease by 1 while β would increase by 0.2. When α decreased to 1, the decrease step of α was changed to 0.1. Eventually, when α decreased to 0, β increased to 1.5, and the success rate exceeded 90% after one minute, the decoder's update stopped and it started to collect data. In the task of feedforward BMI, when α decreased to 0, β increased to 1.5, the ring would appear and β decreased to 1. In this process, the BMI system kept collecting movement intention and updating. If the success rate was higher than 70% after one minute, the recalibration was finished and the task paradigm was changed to interception. Again, if the success rate was higher than 70% after one minute, the recalibration was finished and it started to collect data.

Feedforward BMI performance evaluation

Three kinds of performance metrices for BMI were used in the present study: success rate, time to target and path efficiency. Time to target was defined as the time from the start of brain control to when the cursor reached the target. The path efficiency was calculated according to equation 11:

$$PF = \frac{\left\|\boldsymbol{p}_{target} - \boldsymbol{p}_{center}\right\|_2}{Traj_{cursor}} \quad 11$$

where || || denoted the L_2 norm, $\boldsymbol{p}_{target}$ was the position of the target, $\boldsymbol{p}_{center}$ was the position of screen center, and the $Traj_{cursor}$ was the length of the cursor's trajectories in a trial. All the performance metrices were calculated in one session with the exclusion of trials during the decoder's initialization and recalibration.

Neural representation analysis

Raw neural signals were spike-sorted to obtain isolated units, and peri-event time histograms (PETHs) of each unit were calculated with spike trains aligned to corresponding event, binned into 20-ms window and then smoothed with a Gaussian kernel (SD=60 ms). Three events were used with the duration being 2000 ms: target onset (TO) ±1000 ms, Go signal (GO) ±1000 ms, and movement onset (MO)±1000 ms. Firing rates were averaged across trials according to the final eight movement-directions, and the preferred direction in each bin was estimated using:

$$F = Acos(\theta - \theta_{PD}) + b \quad 12$$

where F was the firing rate, A was the tuning depth, θ was the arm movement direction or the cursor's ballistic direction, θ_{PD} was the estimated preferred direction, and b was the baseline. $|\Delta\theta_{PD}|$, the absolute difference of preferred direction between two epochs, was defined according to equation 13:

$$|\Delta\theta_{PD}| = \begin{cases} |\theta_1 - \theta_2|, & |\theta_1 - \theta_2| < \pi \\ \left||2\pi - |\theta_1 - \theta_2|\right|, & |\theta_1 - \theta_2| \geq \pi \end{cases} \quad 13$$

where θ_1 and θ_2 were preferred directions in two epochs.

Neural activity decomposition analysis

A dataset of population activities was constructed. All neurons' firing rates which were preprocessed as described earlier were first normalized, demeaned across all the trials, then averaged according to the eight final arm movement or ballistic directions to obtain a matrix of $N \in \mathbb{R}^{k \times n \times t}$, where k denoted the condition number, n denoted the number of neurons, and t denoted the number of time bins. Then N was reshaped into matrix $M \in \mathbb{R}^{k \times n * t}$, performed with principal component analysis (PCA), and the eigenvectors of top three PCs were selected to construct the feature space. Neural trajectories were obtained by projecting the vectors of matrix N in the same arm movement or ballistic direction in each time point onto the space and then concatenating them.

The overlapping extent of preparatory and execution subspaces was estimated by calculating the alignment index (Elsayed et al., 2016). M_{prep} and M_{exec} were matrixes of population neural activities in preparatory and execution epochs, respectively, which came from matrix M except that they were aligned to the movement onset (M_{prep}: -300 ms to -280 ms, M_{exec}: 180 ms to 200 ms).

C_{prep} and C_{exec}, termed as the preparatory and execution subspace, respectively, were constructed by two sets of the first ten PCs after performing PCA on M_{prep} and M_{exec}, and the alignment index between them was calculated according to:

$$Alignment\ index = \frac{Tr\left(C_{exec}^{T}\Sigma_{prep}C_{exec}\right)}{\sum_{i=1}^{10}\sigma_{prep}^{i}} \quad 14$$

where Σ_{prep} denoted the covariance matrix and σ_{prep}^{i} denoted the eigenvalue in the preparatory epoch. Variances of population activities captured during the preparatory and execution epochs were calculated by projecting these activities onto the corresponding subspaces. Population activities in the preparatory and execution epochse were also projected onto the Stiefel manifold, and the corresponding subspaces of this manifold were computed using pymanopt (Elsayed et al., 2016). The alignment indexes of the control group in Fig. 3d and h were from 20 sets of data randomly generated.

jPCA projection and CCA analysis

For neurons recorded during the brain-controlled movements represent the cursor movement state was very sparse, the neurons were selected according to the R^2(or the goodness-of-fit, method) and concatenated across several sessions for jPCA projection (time window: -100 to 300 ms around MO).

In the present study, jPCA, a dimensionality reduction method identifying low-dimensional rotating subspaces of neural population activities over time (Churchland et al., 2012) was used. Spike trains aligned to movement onset (arm movement: -50 ms to 150 ms, brain control: -100 ms to 300 ms) were processed as follows: binned into 2-ms windows, smoothed with a Gaussian kernel (SD =60 ms), averaged by movement direction, normalized and reshaped into matrix $S \in \mathbb{R}^{k\times n*t}$. jPCA subspaces were computed by fitting using $\dot{S} = M_{skew}S$, and neural trajectories were obtained by projecting S onto the first two PCs' spanned subspace with each trajectory representing a movement direction, red and green denoting distinct rotational directions, and solid circles and arrows marking the start and end states of neural dynamics, respectively.

In the canonical correlation analysis, firing rates in arm movement and brain control, calculated with spike trains which were aligned to movement onset (-300 ms to 400 ms), binned into 20-ms windows, smoothed with a Gaussian kernel (SD = 60 ms), were organized into matrixes N_{hand} and N_{cursor}, respectively. Q_{hand}, Q_{cursor}, R_{hand}, and R_{cursor} were obtained after the QR decomposition of N_{hand} and N_{cursor}. Aligned neural manifolds (M_{hand} and M_{cursor}), were computed via singular value decomposition of $Q_{hand}^{T}Q_{cursor}$, yielding $U\Sigma V^{T}$, and then based on the equations $M_{hand} = N_{hand}^{-1}U$, $M_{cursor} = N_{cursor}^{-1}V$. The aligned neural data, resulting from projecting matrixes N_{hand}和N_{cursor} onto their corresponding neural manifolds, were used for CCA (Safaie et al., 2023).

Supplementary

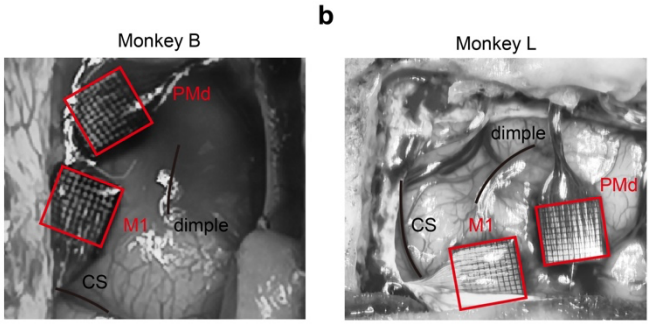

Supplementary Fig. S1 Implantations of Utah arrays into the motor cortex. Two Utah arrays implanted into the dorsal premotor cortex (PMd) and primary cortex (M1), respectively, were marked with red squares in the pictures. Central sulcus and dimple were marked with black lines to indicate the referenced landmarks for implantation.

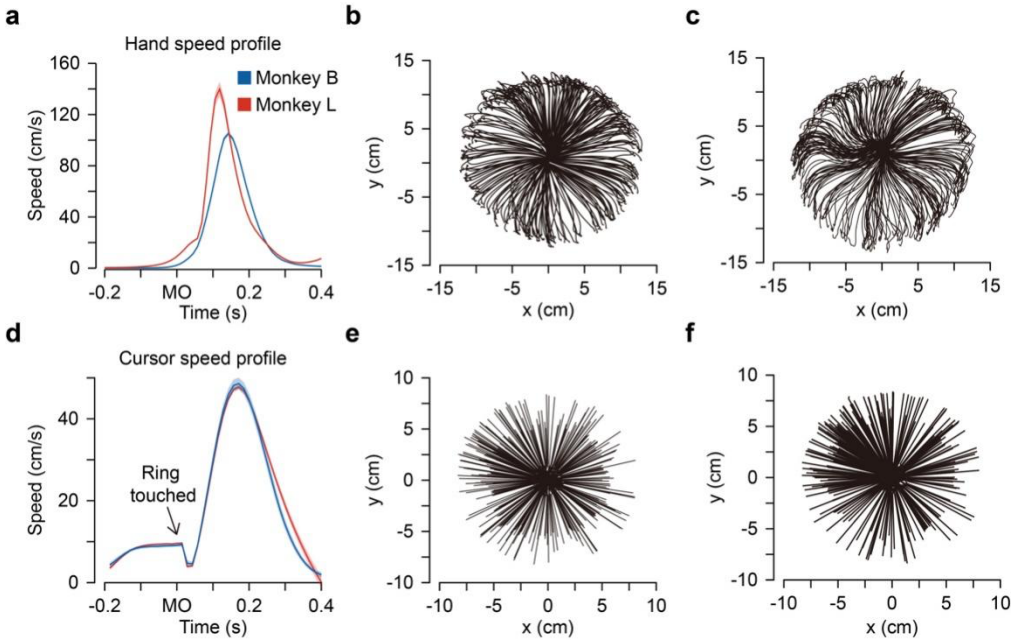

Supplementary Fig. S2. Trajectories of hand and cursor. (a) A marker on one finger of the monkey was labeled to track the trajectories of hand movement. Time point '0' was aligned to the onset of arm movement. (b-c) Hand movement trajectories in manual interception task. Time window: from the go-cue onset to target touching (panel b for monkey B, and c for monkey L). (d) Ballistic velocity profile of the cursor. Time point '0' was aligned to the time when the cursor touched the ring. (e-f) Cursor movement trajectories in feedforward BMI task. Time window: from the onset that the cursor could be operated to the time when the cursor touched the target. (panel e for monkey B, and f for monkey L).

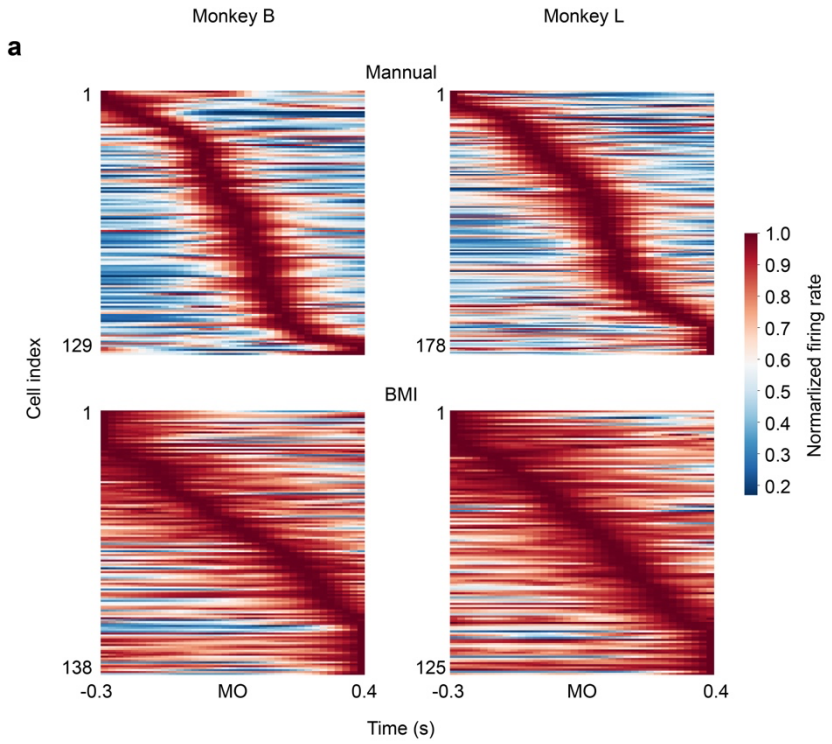

Supplementary Fig. S3. Heatmaps of normalized firing rates after being averaged across all the trials for single units in the arm movement (upper panels) and brain control (bottom panels) for both monkeys. Neural activities were aligned to movement onset (MO), with units sorted with the time of peak firing rate.

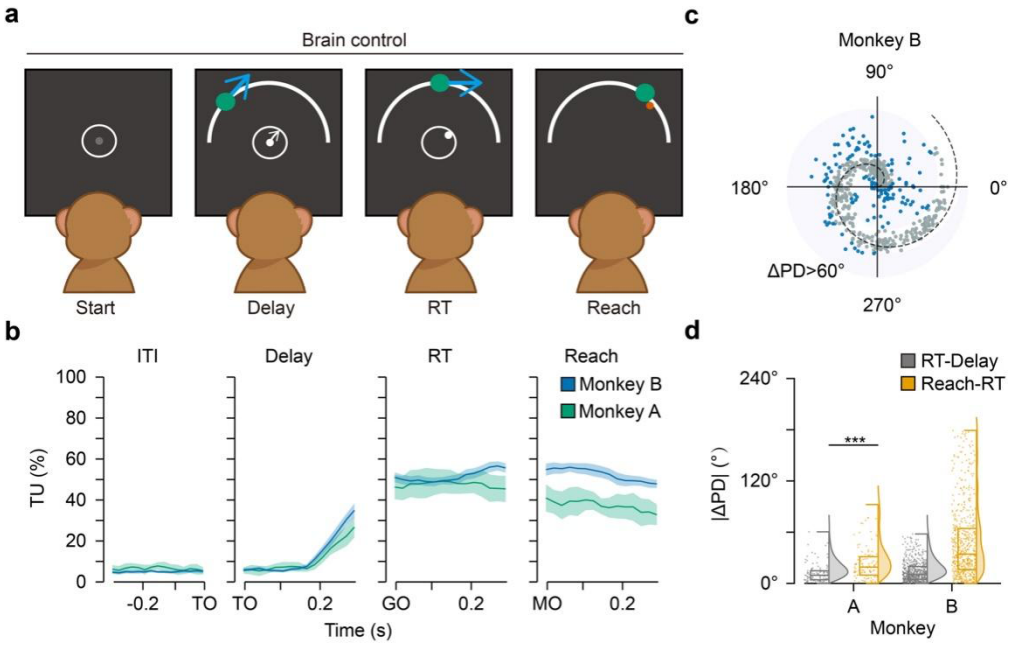

Supplementary Fig. S4. Tunings of single units under the occlusion condition (i.e. ballistic cursor was occluded in the execution epoch). (a) The schematic of the BMI paradigm, with cursor disappearing during its ballistic flight epoch. (b) Tuned unit's percent (TU%) in different epochs when aligned to the onset of target on (TO), Go signal on (GO), and movement onset (MO) in the occlusion condition. (c) Plot shows the preferred directions (PD) in the planning and execution epoch each neuron in a polar coordinate system. The grey dashed line shows coordinates of neurons with the same PD in the two epochs, and blue dots represent neurons whose PD difference was larger than 60º. (d) Absolute differences of PD between planning and delay epochs and between execution and delay epochs for both monkeys.

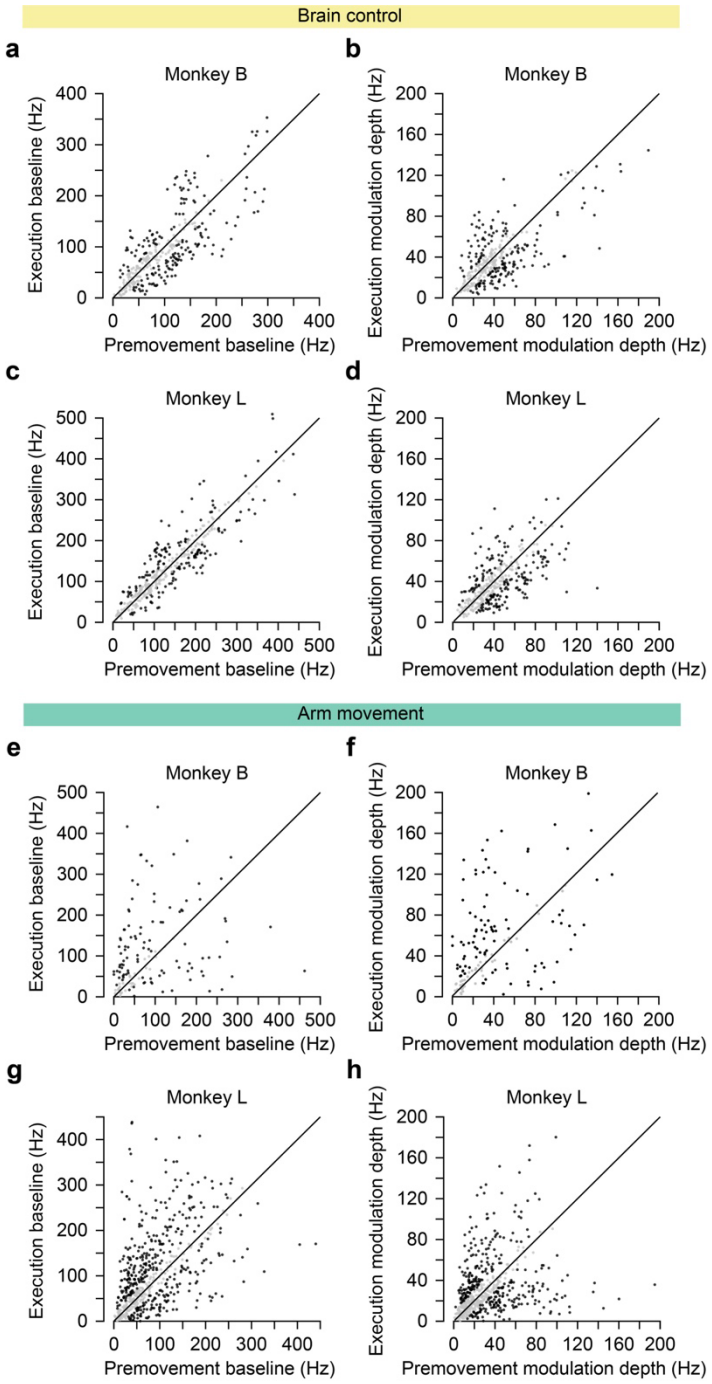

Supplementary Fig. S5. Firing rates of 'baseline' neurons and 'modulation depths' neurons in planning epoch (-200 ms to -180 ms, aligned to MO) and execution epoch (180 ms to 200 ms, aligned to MO) in the brain control and arm movement conditions for both monkeys. Left column (a-d): brain control; right column (e-h): arm movement. Dark dots represent neurons with significant change of baseline or modulation depth.

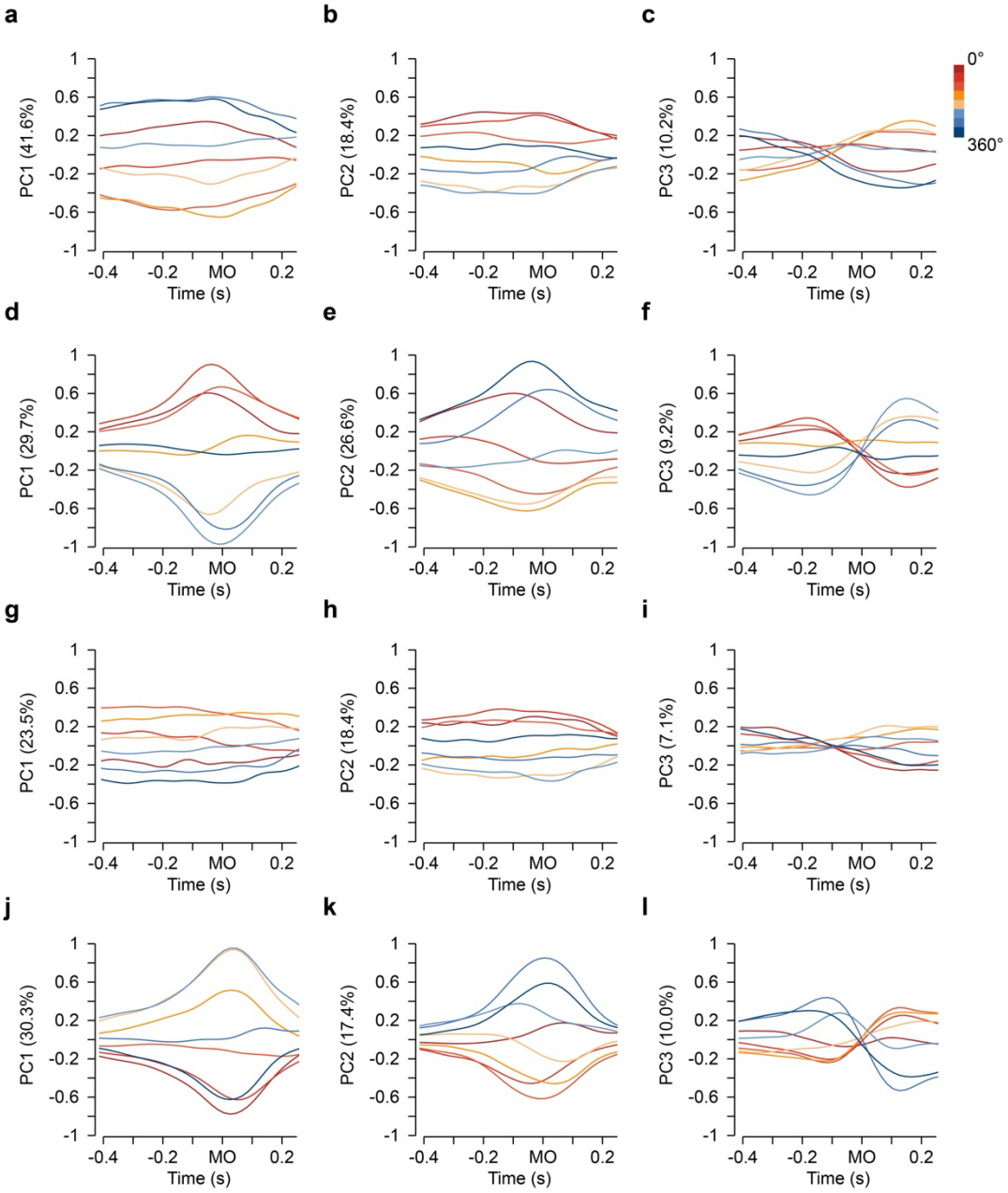

Supplementary Fig. S6. Top three PCs in eight movement directions. The first and second rows were under the brain control and arm movement conditions, respectively, for monkey B. The third and fourth rows were under the brain control and arm movement conditions, respectively, for monkey L.

References

Bensmaia, S. J., & Miller, L. E. (2014). Restoring sensorimotor function through intracortical interfaces: progress and looming challenges. *Nat Rev Neurosci*, *15*(5), 313–325. https://doi.org/10.1038/nrn3724

Churchland, M. M., Cunningham, J. P., Kaufman, M. T., Foster, J. D., Nuyujukian, P., Ryu, S. I., & Shenoy, K. V. (2012). Neural population dynamics during reaching. *Nature*, *487*(7405), 51–56. https://doi.org/10.1038/nature11129

Churchland, M. M., & Shenoy, K. V. (2024). Preparatory activity and the expansive null-space. *Nat Rev Neurosci*, *25*(4), 213–236. https://doi.org/10.1038/s41583-024-00796-z

Degenhart, A. D., Bishop, W. E., Oby, E. R., Tyler-Kabara, E. C., Chase, S. M., Batista, A. P., & Yu, B. M. (2020). Stabilization of a brain-computer interface via the alignment of low-dimensional spaces of neural activity. *Nat Biomed Eng*, *4*(7), 672–685. https://doi.org/10.1038/s41551-020-0542-9

Elsayed, G. F., Lara, A. H., Kaufman, M. T., Churchland, M. M., & Cunningham, J. P. (2016). Reorganization between preparatory and movement population responses in motor cortex. *Nat Commun*, *7*, 13239. https://doi.org/10.1038/ncomms13239

Gallego, J. A., Perich, M. G., Chowdhury, R. H., Solla, S. A., & Miller, L. E. (2020). Long-term stability of cortical population dynamics underlying consistent behavior. *Nature Neuroscience*, *23*(2), 260–270. https://doi.org/10.1038/s41593-019-0555-4

Georgopoulos, A., Kalaska, J., Caminiti, R., & Massey, J. (1982). On the relations between the direction of two-dimensional arm movements and cell discharge in primate motor cortex. *The Journal of Neuroscience*, *2*(11), 1527–1537. https://doi.org/10.1523/jneurosci.02-11-01527.1982

Gilja, V., Nuyujukian, P., Chestek, C. A., Cunningham, J. P., Yu, B. M., Fan, J. M., Churchland, M. M., Kaufman, M. T., Kao, J. C., Ryu, S. I., & Shenoy, K. V. (2012). A high-performance neural prosthesis enabled by control algorithm design. *Nat Neurosci*, *15*(12), 1752–1757. https://doi.org/10.1038/nn.3265

Golub, M. D., Yu, B. M., & Chase, S. M. (2015). Internal models for interpreting neural population activity during sensorimotor control. *Elife*, *4*, e10015. https://doi.org/10.7554/eLife.10015

Kao, J. C., Nuyujukian, P., Ryu, S. I., Churchland, M. M., Cunningham, J. P., & Shenoy, K. V. (2015). Single-trial dynamics of motor cortex and their applications to brain-machine interfaces. *Nat Commun*, *6*, 7759. https://doi.org/10.1038/ncomms8759

Kao, T.-C., Sadabadi, M. S., & Hennequin, G. (2021). Optimal anticipatory control as a theory of motor preparation: A thalamo-cortical circuit model. *Neuron*, *109*(9), 1567–1581.e1512. https://doi.org/https://doi.org/10.1016/j.neuron.2021.03.009

Karpowicz, B. M., Ali, Y. H., Wimalasena, L. N., Sedler, A. R., Keshtkaran, M. R., Bodkin, K., Ma, X., Rubin, D. B., Williams, Z. M., Cash, S. S., Hochberg, L. R., Miller, L. E., &

Pandarinath, C. (2025). Stabilizing brain-computer interfaces through alignment of latent dynamics. *Nature Communications*, *16*(1), 4662. https://doi.org/10.1038/s41467-025-59652-y

Lebedev, M. A., & Nicolelis, M. A. (2017). Brain-Machine Interfaces: From Basic Science to Neuroprostheses and Neurorehabilitation. *Physiol Rev*, *97*(2), 767–837. https://doi.org/10.1152/physrev.00027.2016

Li, Y., Wang, Y., & Cui, H. (2018). Eye-hand coordination during flexible manual interception of an abruptly appearing, moving target. *J Neurophysiol*, *119*(1), 221–234. https://doi.org/10.1152/jn.00476.2017

Orsborn, A. L., Moorman, H. G., Overduin, S. A., Shanechi, M. M., Dimitrov, D. F., & Carmena, J. M. (2014). Closed-loop decoder adaptation shapes neural plasticity for skillful neuroprosthetic control. *Neuron*, *82*(6), 1380–1393. https://doi.org/10.1016/j.neuron.2014.04.048

Pandarinath, C., Ames, K. C., Russo, A. A., Farshchian, A., Miller, L. E., Dyer, E. L., & Kao, J. C. (2018). Latent Factors and Dynamics in Motor Cortex and Their Application to Brain–Machine Interfaces. *The Journal of Neuroscience*, *38*(44), 9390. https://doi.org/10.1523/JNEUROSCI.1669-18.2018

Pandarinath, C., & Bensmaia, S. J. (2022). The science and engineering behind sensitized brain-controlled bionic hands. *Physiological Reviews*, *102*(2), 551–604. https://doi.org/10.1152/physrev.00034.2020

Perich, M. G., Narain, D., & Gallego, J. A. (2025). A neural manifold view of the brain. *Nat Neurosci*, *28*(8), 1582–1597. https://doi.org/10.1038/s41593-025-02031-z

Safaie, M., Chang, J. C., Park, J., Miller, L. E., Dudman, J. T., Perich, M. G., & Gallego, J. A. (2023). Preserved neural dynamics across animals performing similar behaviour. *Nature*, *623*(7988), 765–771. https://doi.org/10.1038/s41586-023-06714-0

Shenoy, K. V., Sahani, M., & Churchland, M. M. (2013). Cortical control of arm movements: a dynamical systems perspective. *Annu Rev Neurosci*, *36*, 337–359. https://doi.org/10.1146/annurev-neuro-062111-150509

Stavisky, S. D., Kao, J. C., Ryu, S. I., & Shenoy, K. V. (2017). Motor Cortical Visuomotor Feedback Activity Is Initially Isolated from Downstream Targets in Output-Null Neural State Space Dimensions. *Neuron*, *95*(1), 195–208 e199. https://doi.org/10.1016/j.neuron.2017.05.023

Suway, S. B., Orellana, J., McMorland, A. J. C., Fraser, G. W., Liu, Z., Velliste, M., Chase, S. M., Kass, R. E., & Schwartz, A. B. (2018). Temporally Segmented Directionality in the Motor Cortex. *Cereb Cortex*, *28*(7), 2326–2339. https://doi.org/10.1093/cercor/bhx133

Velliste, M., Perel, S., Spalding, M. C., Whitford, A. S., & Schwartz, A. B. (2008). Cortical control of a prosthetic arm for self-feeding. *Nature*, *453*(7198), 1098–1101. https://doi.org/10.1038/nature06996

Zhang, Y., Chen, Y., Wang, T., & Cui, H. (2025). Neural Geometry from Mixed Sensorimotor Selectivity for Predictive Sensorimotor Control. In: eLife Sciences Publications, Ltd.